Publication Year	2015
Acceptance in OA@INAF	2020-04-10T14:39:08Z
Title	The Signature of Flare Activity in Multifractal Measurements of Active Regions Observed by SDO/HMI
Authors	GIORGI, Fabrizio; ERMOLLI, Ilaria; ROMANO, Paolo; STANGALINI, MARCO; Zuccarello, Francesca; et al.
DOI	10.1007/s11207-014-0609-4
Handle	http://hdl.handle.net/20.500.12386/23991
Journal	SOLAR PHYSICS
Number	290

Solar Physics
DOI: 10.1007/•••••-•••-•••-••••-•

The Signature of Flare Activity in Multifractal Measurements of Active Regions Observed by SDO/HMI

F. Giorgi[1] · **I. Ermolli**[1] · **P. Romano**[2] · **M. Stangalini**[1] · **F. Zuccarello**[3] · **S. Criscuoli**[4]

© Springer ••••

Abstract Recent studies indicate that measurements of fractal and multifractal parameters of active regions (ARs) are not efficient tools to discriminate ARs on the basis of the flare activity, as well as to predict flare events. Attempting validation of this result on a large data set of higher spatial and temporal resolution, as well as higher flux sensitivity, observations than employed in previous studies, we analyzed high-cadence time series of line-of-sight magnetograms of 43 ARs characterized by different flare activity, which were observed with SDO/HMI from May 2010 to December 2013. On these data, we estimated four parameters, the generalized fractal dimensions D_0 and D_8, and the multifractal parameters $C_{\rm div}$ and $D_{\rm div}$. We found distinct average values of the parameters measured on ARs that have hosted flares of different class. However, the dispersion of values measured on ARs that have produced same class events is such that the parameters deduced from distinct classes of flaring regions can also largely overlap. Based on the results of our measurements, C- and M-class flaring ARs are practically indistinguishable, as well as M- and X-class flaring ARs. We found consistent changes on the time series of the measured parameters only on $\approx 50\%$ of the studied ARs and $\approx 50\%$ of the M- and X-class events considered. We show that these results hold for fractal and multifractal parameter estimates based on both total unsigned and signed flux data of the analyzed ARs.

Keywords: Flares, forecasting; Flares, relation to magnetic field; Magnetic fields, photosphere

[1] INAF Osservatorio Astronomico di Roma, via Frascati 33, 00040 Monte Porzio Catone, Italy
email: giorgi@oaroma.inaf.it
[2] INAF - Osservatorio Astrofisico di Catania, Via S. Sofia 78, 95125 Catania, Italy
[3] Dipartimento di Fisica e Astronomia - Sezione Astrofisica, Università di Catania, Via S. Sofia 78, 95125 Catania, Italy
[4] National Solar Observatory Sacramento Peak P.O. Box 62 Sunspot, NM 88349-0062, United States

arXiv:1705.06708v1 [astro-ph.SR] 18 May 2017

1. Introduction

Solar flares are among the most energetic events in the solar system. They occur in active regions (ARs), by involving processes at various heights in the solar atmosphere that are powered by the magnetic field (Shibata and Magara, 2011). Observations show that the photospheric topology of magnetic field is one of the key factors in determining the evolution of ARs. There is a general trend for large regions to produce large flares, and for more complex regions to generate more numerous and larger flares than other regions of comparable size (Sammis, Tang, and Zirin, 2000). Emergence of a bipolar region that interacts with preexisting magnetic field in the corona, and activation of a filament with destabilization in the subsisting magnetic region, are known as precursors events preceding the onset of flares. However, the precise conditions required to create the enormously energetic (up to 10^{32} erg on the timescale of hours) flare events are as yet unknown (Leka and Barnes (2013), and references therein). Because interplanetary disturbances associated with solar flares can impact space- and ground-based infrastructures, identification of precursor conditions leading to solar flares is getting a growing interest for practical applications of space weather forecast (Hapgood, 2012).

Any measurement of magnetic energy and complexity in an AR deserves interest for testing its sensitivity to single out the flare activity of the region for space weather forecasts. However, among the various measurements, those concerning multifractal properties of the region in the photosphere have the potential of providing information about the interaction between magnetic field and plasma motions that may lead to flare events. Indeed, these parameters are thought to describe AR properties that can be consequence of a self-organized evolution (see discussion by *e.g.* Georgoulis, 2012).

Several studies in the literature indicate that measurements of fractal and multifractal properties of ARs may help assessing the eruptive potential of the regions and also predicting their flare activity (for a list of studies carried out during the last decade see *e.g.* Ermolli *et al.* (2014), hereafter Paper I). Nevertheless, the literature also shows conflicting conclusions on the efficiency of these measurements to discriminate flaring ARs. For example, McAteer, Gallagher, and Ireland (2005) reported no discernible differences between the fractal dimension distributions of different Mount Wilson classes of ARs that were studied on *Solar and Heliospheric Observatory* (SOHO)/*Michelson-Doppler Imager* (MDI; Scherrer *et al.*, 1995) line-of-sight (LOS) magnetograms. However, they also showed that there is a good correlation between the increased flare productivity of ARs, in terms of both flare size and frequency, and increased fractal dimension measured in the ARs. Besides, they identified a lower threshold fractal dimension value which an AR must possess in order to have the potential to produce an M-class (X-class) flare. More recently, Georgoulis (2012) reported that none of the widely-used multifractal parameters measured in his study on a large data set of SOHO/MDI LOS magnetograms allows to distinguish AR with major flares from flare-quiet ones, though both classes of solar regions show significant fractality and multifractality. Then, from analysis of higher resolution observations than employed in the previous study, Georgoulis (2013) also found that the multiscale

parameters measured on *Solar Dynamics Observatory* (SDO)/*Heliospheric and Magnetic Imager* (HMI; Scherrer *et al.*, 2012; Schou *et al.*, 2012; Wachter *et al.*, 2012) LOS magnetograms of an intensely eruptive AR and of a flare-quiet AR have fairly similar values and temporal evolutions.

Recent results from an analysis of near-simultaneous observations of a flaring AR by SOHO/MDI and SDO/HMI (Paper I) suggested us to further investigate the response of the fractal and multifractal parameters to the flare activity of ARs. In particular, Paper I shows that the measurements derived from SOHO/MDI observations are affected by larger and spurious variations over time than those deduced from analysis of the higher-quality SDO/HMI data. Therefore, analysis of higher quality observations of a larger sample of ARs than analyzed by Georgoulis (2013) may produce measurements of the multifractal parameters characterized by a significantly reduced dispersion than derived by Georgoulis (2012). The study presented herein investigates the possibility that a reduced dispersion of multifractal parameters measured on SDO/HMI observations of ARs may help discriminating flaring from flare-quiet regions. To this purpose, we analyzed time series of magnetograms of 43 ARs with different flare activity that were observed with SDO/HMI from May 2010 to December 2013. We also noticed that almost all the studies of multifractal properties in flaring ARs were carried out on the total unsigned flux measurement of the regions, which is considered a standard-flare forecasting tool (Barnes and Leka, 2008). To the knowledge of these authors, only Georgoulis (2005) reported that discriminating between the two polarities in the studied ARs do not alter the results derived from analysis of total unsigned flux measurements of ARs. New observational evidences on the physical mechanisms driving the evolution of magnetic field in more flaring ARs, concerning *e.g.* the photospheric magnetic flux change and cancellation (Burtseva and Petrie, 2013; Cliver, Petrie, and Ling, 2012) and the fragmentation of magnetic helicity patches (Romano and Zuccarello, 2011), suggested us to study multifractal parameters inside ARs, by taking into account the evolution of magnetic regions with different polarities, thus using signed magnetic flux measurements for multifractal parameters estimates rather than total unsigned flux data. It has been also shown that the regions with different polarity in an AR have distinct morphology (see *e.g.* Yamamoto, 2012) and dynamical behavior (Giannattasio *et al.*, 2013). Therefore, we also tested the response of measurements of multifractal parameters based on signed flux measurements to the flare activity of the ARs.

The paper is organized as follows. The data sets and analysis methods employed in our study are described in Section 2. Our main findings are presented in Section 3, whereas the conclusions of this study are summarized in Section 4.

2. Data and Methods

We analyzed 43 ARs characterized by different flare activity that were observed by SDO/HMI from May 2010 to December 2013. Table 1 lists the ARs in our sample, by providing information about the flare events hosted by the region and its flaring level. The latter is described by the flare index (FI; Li *et al.*, 2004),

Table 1. ARs analyzed in this study accordingly to the NOAA catalog, with the number of B-, C-, M-, and X-class events hosted by the region during its transit over the solar disc, the flare index (FI) computed during the same time interval and the maximum value of the flare index (FI max) for the most intense event produced by the region. The FI values are given using $\times 10^{-3}$ erg $cm^{-2}s^{-1}$ units. Details are given in the text. Date (year, month, day) and time (hour, minutes) indicate the AR transit at the central meridian, while Hem is the solar hemisphere hosting the AR. M- and X-class flaring ARs are marked bold.

AR	B	C	M	X	FI	FI max	date	time (UT)	Hem
11072	6	0	0	0	1.3	0.7	2010 05 23	00:24	S
11117	55	5	0	0	28.1	5.7	2010 10 25	19:24	N
11143	2	0	0	0	0.6	0.4	2011 01 08	22:24	S
11146	2	0	0	0	0.4	0.2	2011 01 14	14:48	N
11158	6	54	7	1	615.6	220.0	2011 02 13	23:59	S
11166	7	25	4	1	303.6	150.0	2011 03 08	20:24	N
11283	10	16	5	2	602.7	210.0	2011 09 05	20:24	N
11318	0	1	0	0	1.4	1.4	2011 10 12	17:24	N
11429	3	47	15	3	1342.6	540.0	2012 03 08	22:48	N
11504	8	42	5	0	178.9	19.0	2012 06 15	00:24	S
11513	8	25	7	0	205.7	28.0	2012 07 02	04:24	N
11515	5	77	24	0	1064.1	69.0	2012 07 02	23:24	S
11520	1	32	8	1	444.3	140.0	2012 07 12	11:36	S
11536	2	20	4	0	166.3	61.0	2012 08 01	11:24	S
11613	1	21	5	0	184.9	60.0	2012 11 16	01:36	S
11618	5	23	5	0	152.8	35.0	2012 11 21	17:00	N
11640	7	6	0	0	15.9	4.0	2013 01 01	05:24	N
11652	3	23	3	0	96.9	17.0	2013 01 11	23:24	N
11660	13	3	0	0	16.4	5.8	2013 01 20	17:24	N
11663	5	1	0	0	2.8	1.1	2013 01 30	04:36	S
11667	19	6	0	0	34.8	8.7	2013 02 07	08:24	N
11670	13	3	0	0	10.2	1.5	2013 02 09	21:00	N
11675	9	5	1	0	31.6	19.0	2013 02 19	06:24	N
11689	5	3	0	0	7.2	2.2	2013 03 10	08:48	S
11691	8	1	0	0	6.8	2.1	2013 03 12	08:12	N
11692	15	14	2	0	64.1	16.0	2013 03 15	22:00	N
11696	6	7	0	0	12.2	1.4	2013 03 14	12:36	N
11708	10	2	0	0	8.4	2.7	2013 04 03	00:24	N
11719	10	16	2	0	125.3	65.0	2013 04 12	08:36	N
11726	16	72	1	0	194.5	10.0	2013 04 20	14:24	N
11731	1	35	3	0	115.0	14.0	2013 04 30	21:36	N
11734	2	27	0	0	51.0	3.4	2013 05 05	01:36	S
11739	2	28	2	0	149.8	57.0	2013 05 09	04:24	N
11756	5	15	0	0	34.6	3.9	2013 05 25	21:24	S
11778	3	11	1	0	65.1	29.0	2013 06 28	22:36	S
11863	1	0	0	0	0.0	0.0	2013 10 10	14:48	S
11868	0	2	0	0	4.9	2.9	2013 10 18	02:36	N
11875	1	66	11	2	829.8	230.0	2013 10 23	09:24	N
11882	0	10	13	2	695.6	210.0	2013 10 30	10:24	S
11890	2	51	5	3	840.2	330.0	2013 11 08	18:00	S
11896	0	1	0	0	1.9	1.9	2013 11 16	20:24	N
11918	0	4	0	0	7.3	2.2	2013 12 14	18:24	S
11923	1	0	0	0	0.0	0.0	2013 12 12	22:24	N

which was computed assuming the flare history of the region depicted by the NOAA's GOES X-ray archive during the disc transit of the region, as well as by considering the most intense event hosted by the region (hereafter referred to as maximum FI, FI max). FI max is employed in the following to discriminate the analyzed ARs depending on their flaring activity. In particular, the X-, M-, and B or C-class flaring ARs discussed below correspond to the regions whose FI max>100, 10<FI max<100, and FI max<10, respectively.

The AR sample analyzed in our study contains 22 regions that have hosted $\geq$ M-class flares and 21 regions that have produced from a single B-class to a few B- or C-class events. The analyzed ARs include all the regions observed from February 2011 to December 2013 that have produced either M- or X-class flares, with the disc position specified in the following, and 17 ARs that were either flare-quiet (FI max<1) or less flaring (10<FI max<100) than the flaring regions, observed over the time interval and disc position of the flaring ARs. The sample also contains 4 flare-quiet ARs observed from May 2010 to January 2011, which were considered for comparison with results of earlier studies.

According to the data and methods applied in Paper I, the selected ARs were analyzed using the time series of SDO/HMI Level 1.5 LOS full-disc magnetograms when the AR longitudinal distance was within $\pm 30^\circ$ of the central meridian. The whole data set consists of 20571 magnetograms, each of 4096 $\times$4096 pixels, with a pixel size of 0.505 arcsec and cadence of 720 s. The spatial resolution is set by the instrument aperture to 1 arcsec. The data set was processed as described in Paper I. The main steps are summarized below, following the description given in the original paper.

From each magnetogram, we extracted a sub-array centered on the AR baricenter, whose size slightly exceeds 512$\times$512 pixels. On these data, according to results presented in Paper I and other studies in the literature (*e.g.* Georgoulis, 2012), geometrical projection effects were not compensated for. Indeed, Paper I shows that additional de-projection correction only slightly alter the fractal and multifractal values obtained for the AR, with differences of measurement results that are well within uncertainties of values. However, it is worth noting that the geometrical de-projection of the data does not allow one to recover the loss of spatial resolution due to the increasing solar area subtended by the resolution element of the recording device when one moves from the disc center to the limb. This resolution loss cannot be compensated for when estimating the fractal and multifractal parameters, but it can be minimized with restriction of the AR positions analyzed. These considerations motivate the restriction of our analysis to un-projected ARs with longitudinal distance within $\pm 30^\circ$ of the central meridian.

On each sub-array, we computed the four parameters describing the fractal and multifractal properties of the photospheric magnetic field: the generalized fractal dimension D_0 and D_8, and the multifractal Contribution Diversity $C_{\rm div}$ and Dimensional Diversity $D_{\rm div}$. These parameters are extensively described by *e.g.* McAteer, Gallagher, and Ireland (2005), Criscuoli *et al.* (2009), Georgoulis (2012), and in Paper I. We investigated the variation of these parameters with respect to the flare activity of the analyzed ARs, by considering results derived

from both the unsigned and signed flux measurements of the photospheric magnetic field in the observations. The parameters were computed on the region of interest derived from application of a threshold in the line-of-sight field component in each sub-array. According to results in Paper I, the threshold values employed are ± 3 times the standard deviation of quiet sun measurements in the data, specifically ± 20 G (gauss). All the sub-arrays employed in our study are unaffected by flux saturation.

The accuracy of the methods and algorithms employed in our study, as well the effects on the measured values of using different thresholds for the analysis, are discussed in Paper I. The uncertainty associated with the measured values is equal to the 2-sigma uncertainty for the parameters derived as in Paper I. This uncertainty is shown in *e.g.* Figure 1, for the results of the parameter measurements from unsigned flux data of the analyzed ARs.

3. Results

We focussed our attention on the time series of the various parameters measured on the analyzed ARs. Figures 1 and 2 show a sample of the analyzed data, which correspond to the time series of some among the most flaring ARs in the data set. We first studied the main features of these series, aiming at investigating the possibility that a reduced dispersion of the parameters measured on SDO/HMI observations may improve the efficiency of these measurements to discriminate flaring from flare-quiet regions with respect to previous reports in the literature. Section 3.1 presents the average values of the parameters derived from unsigned flux data of the analyzed ARs, in close analogy to previous results in the literature, whereas Section 3.2 shows the findings from the analysis of the signed flux data of the analyzed regions, aiming at singling out effects of flux discrimination on measurement results. Section 3.3 presents the main features of the temporal evolution of the parameters measured from both unsigned and signed flux data of the studied regions, aiming at highlighting any distinctive patterns in the time series that can be associated with the flaring activity.

3.1. Average Values of the Parameters from Unsigned Flux Data

Figure 3 shows the time series of fractal and multifractal parameters derived from total unsigned flux measurements of the analyzed ARs. In order to point out the dependence of measured values on the AR flaring activity, the results were divided into three groups, according to the three classes of flaring ARs introduced in Section 2. The three classes concern the ARs that have hosted B- or C-class, M-class, and X-class events.

Figure 3 shows that the D_0 values measured on all ARs range between $\approx$ 1.50 and $\approx$ 1.90, in agreement with previous reports in the literature on a significant fractality of the morphology of the magnetic flux concentration in both flaring and flare-quiet ARs (see *e.g.* McAteer, Gallagher, and Ireland (2005), Conlon *et al.* (2008), Criscuoli *et al.* (2009), and Georgoulis (2012) for results of the fractal dimension estimate of ARs derived from the box-counting method

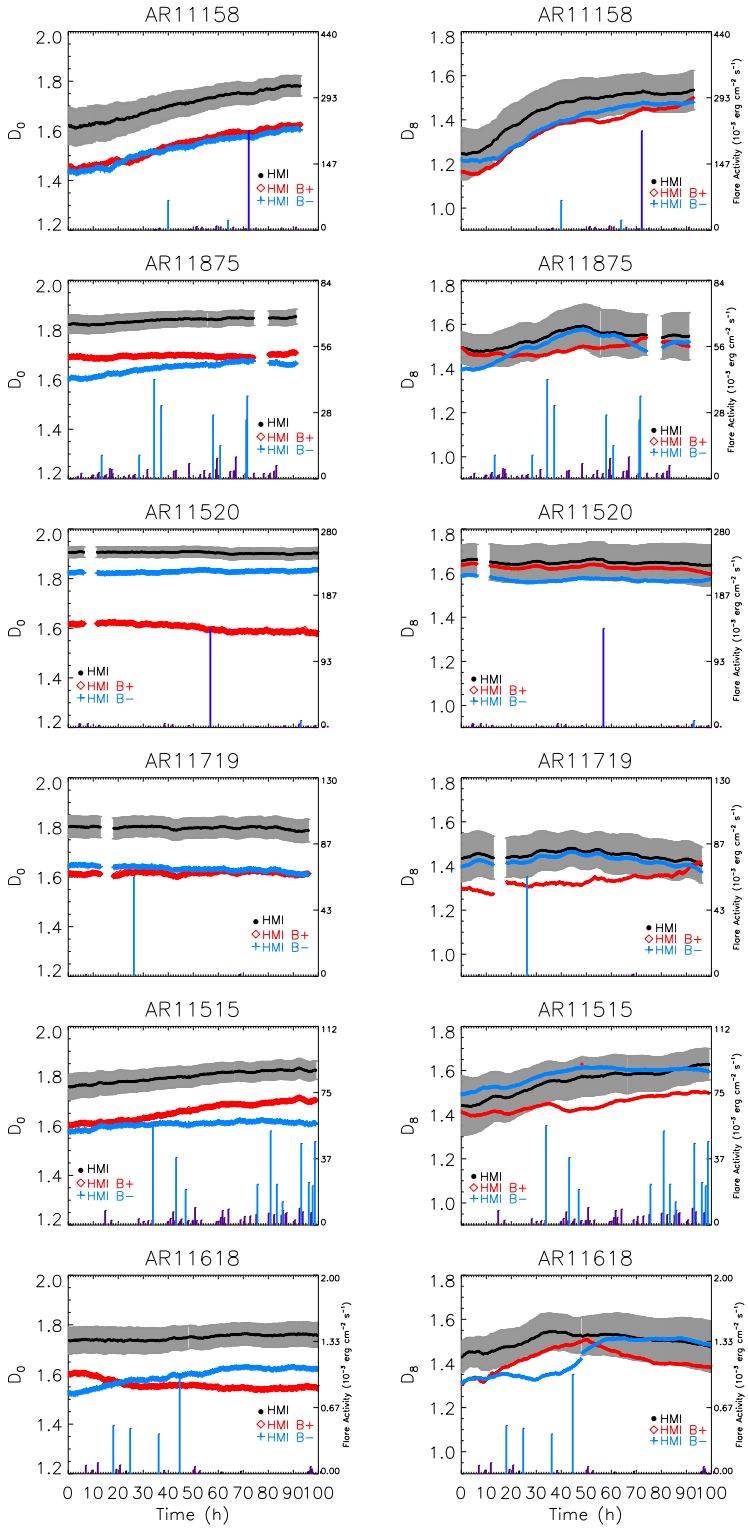

Figure 1. Time series of the fractal parameters D_0 (left) and D_8 (right) measured on six ARs, by considering both unsigned (HMI, black circles) and signed (HMI B+ and HMI B-, red diamonds and blue crosses, respectively) flux data in the analyzed regions. ARs NOAA 11158, 11520, and 11515 appeared in the southern hemisphere, while ARs NOAA 11875, 11719, and 11618 in the northern hemisphere. The leading polarity in the ARs is B+ and B- for the regions in the southern and northern hemisphere, respectively. Vertical bars indicate the flare activity of the AR; each single flare produced by the AR is reported with a bar whose length is proportional to the X-ray flux observed by GOES. Reading for these values are given in the right ordinates. Error bars show the uncertainty associated with the measured values, details are given in the text. For clarity, the error bars are only shown for the results from unsigned flux data. The gaps in the time series are due to the lack of SDO/HMI observations.

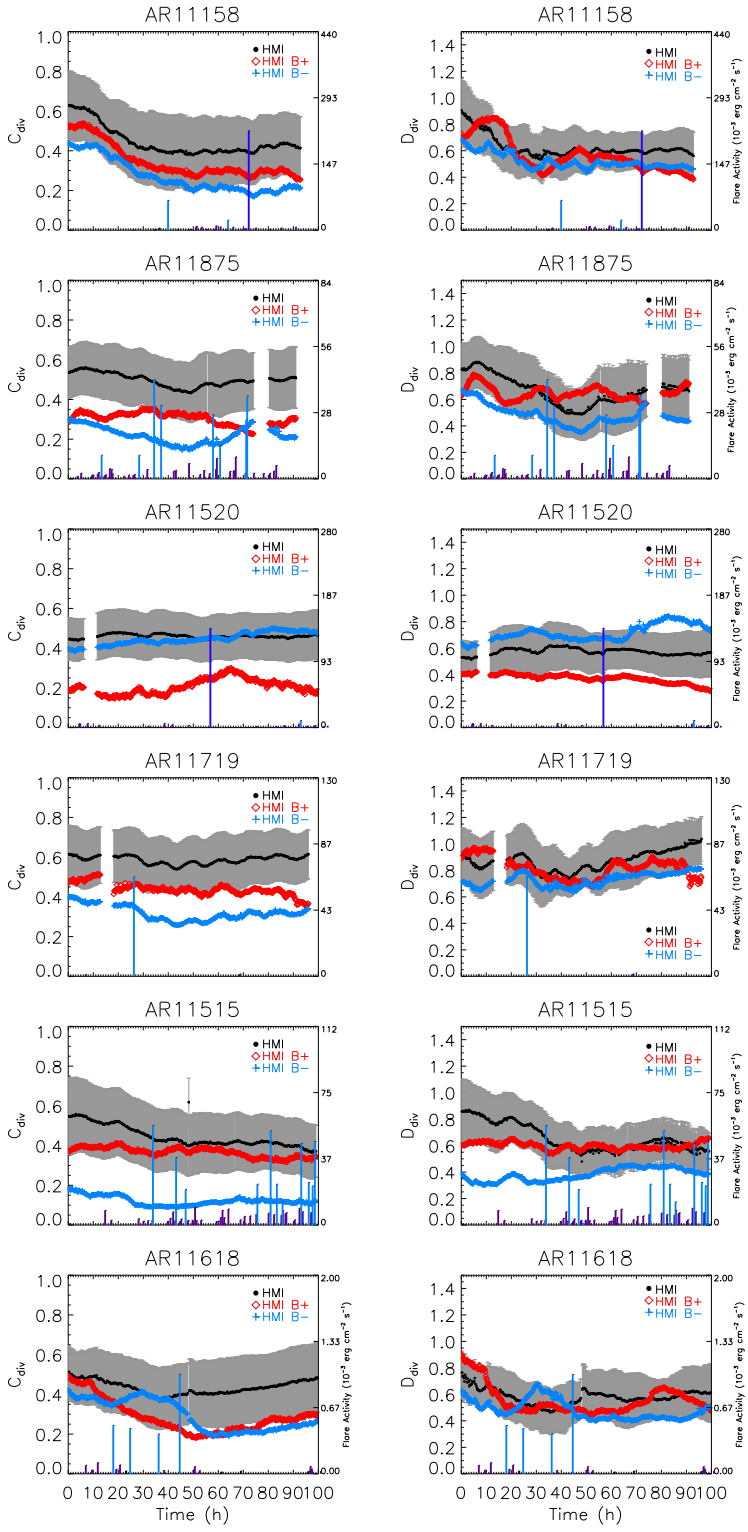

Figure 2. Time series of the multifractal parameters $C_{\rm div}$ (left) and $D_{\rm div}$ (right) measured on six ARs, by considering both unsigned (HMI, black circles) and signed (HMI B+ and HMI B-, red diamonds and blue crosses, respectively) flux data in the analyzed regions. ARs NOAA 11158, 11520, and 11515 appeared in the southern hemisphere, while ARs NOAA 11875, 11719, and 11618 in the northern hemisphere. The leading polarity in the ARs is B+ and B- for the regions in the southern and northern hemisphere, respectively. Error bars and vertical bars as in Figure 1. The gaps in the time series are due to the lack of SDO/HMI observations.

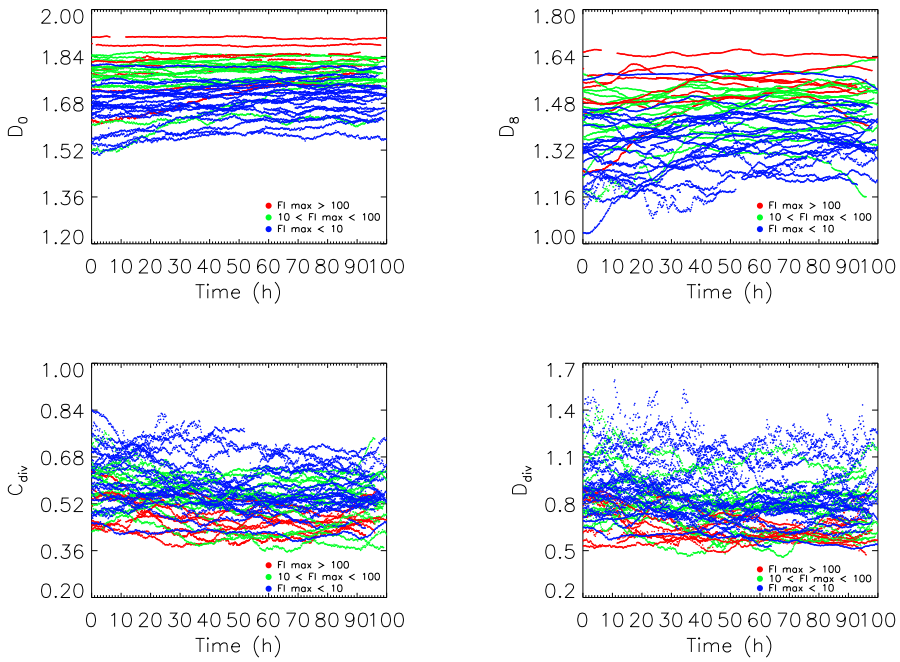

Figure 3. Comparison among results of the fractal and multifractal parameters measured on the whole sample of analyzed ARs by taking into account unsigned magnetic flux data in the studied regions. The time series of fractal parameters D_0 and D_8 (top panels) and multifractal parameters $C_{\rm div}$ and $D_{\rm div}$ (bottom panels) were divided according to the flaring level of the analyzed AR. The results derived from regions that have hosted B- or C- (FI max <10), M- (10< FI max<100), and X- class (FI max>100) flares are shown with blue, green, and red symbols, respectively.

and *e.g.* Criscuoli *et al.* (2007) and references therein for the findings from other methods). Figure 3 also shows that higher D_0 and D_8 values, as well as lower $C_{\rm div}$ and $D_{\rm div}$, are estimated, on average, for the most flaring regions in the AR sample, than derived from the more quiet ARs. We found that the difference between the values derived from the extreme classes of flaring ARs in our sample is larger for the D_0 and D_8 values than for the $C_{\rm div}$ and $D_{\rm div}$ parameters, whose trends obtained from the three classes of analyzed ARs overlap more than for the fractal parameters.

Figure 4 shows the average of the parameters measured on each AR. We found that the parameters derived from the three classes of analyzed ARs are distributed between a lower and an upper limit, but a systematic difference between the trends obtained from distinct classes of flaring ARs seems also to occur. Indeed, Figure 5 shows the relation between the average value of the parameters estimated for each AR in the sample and its FI. The measurements were divided according to the hemisphere hosting the AR, to test any hemispheric signature on them. In agreement with previous works (*e.g.* McAteer, Gallagher, and Ireland, 2005; Abramenko, 2005; Criscuoli *et al.*, 2009), we found that higher values of

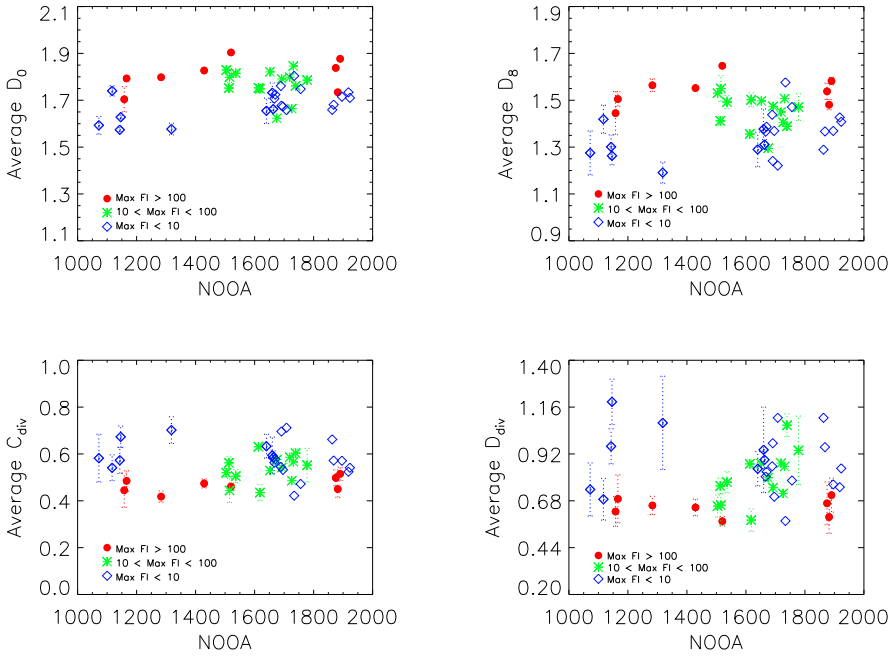

Figure 4. Comparison between the average values of the fractal and multifractal parameters measured on the sample of 43 ARs. Shown are results from unsigned magnetic flux measurements in the AR of the generalized fractal dimension D_0 and D_8 (top panels), and multifractal parameters $C_{\rm div}$ and $D_{\rm div}$ (bottom panels).The regions were divided into three groups according to the flaring level of the studied AR. Details are given in Section 2 and caption of Figure 3.

fractal D_0 and D_8 parameters, as well as a lower value of $C_{\rm div}$ and $D_{\rm div}$, imply a higher flare activity of the ARs, in terms of their FI that account for the flare size and event frequency. The scatter of data does not support the assumption of a linear relation between the compared quantities, although a non-linear relation may hold between them. Figure 5 shows that this result holds likewise for the ARs of both hemispheres.

The results shown in Figures 3 to 5 are quantified in Table 2, which summarizes the average and standard deviation of the parameters measured for each class of analyzed ARs. We found distinct average values of the parameters measured on ARs that have hosted flares of different class. However, the dispersion of values measured on ARs that have produced same class events is such that the parameters deduced from distinct classes of flaring regions can also largely overlap. Based on the results of our measurements, C- and M-class flaring ARs are practically indistinguishable, as well as M- and X-class flaring ARs. However, C- and X-class regions can be either discerned or not depending on the analyzed ARs. These findings give reasons to some conflicting conclusions presented in the literature on the efficiency of the fractal and multifractal measurements to discriminate flaring ARs. In fact, they confirm the statistical trend reported by

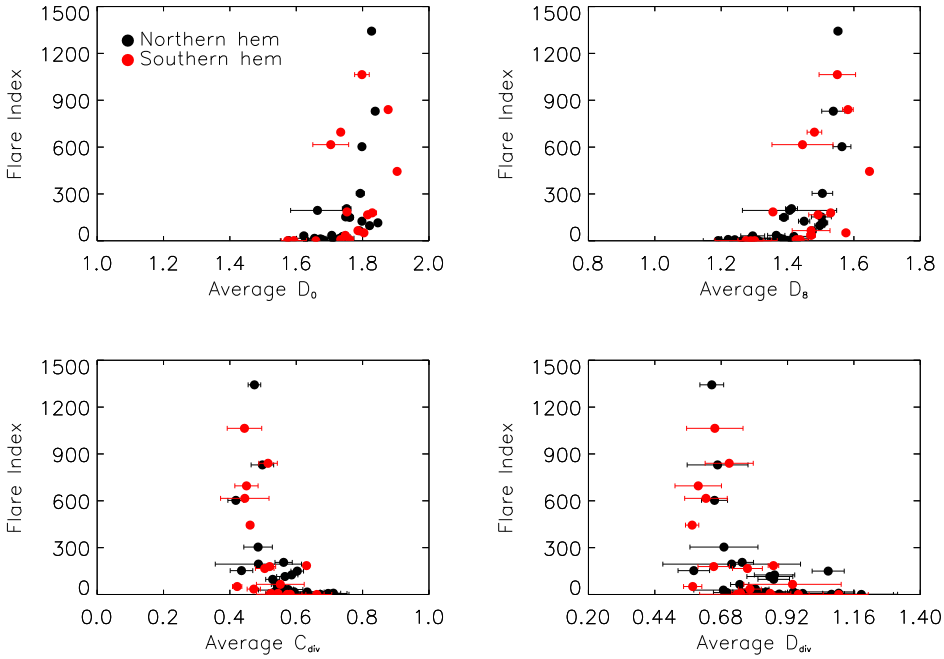

Figure 5. Flare index of the analyzed ARs versus average values of the fractal and multifractal parameters measured on our sample of 43 ARs, which include B- or C-, M-, and X-class flaring regions. Shown are results from unsigned magnetic flux measurements in the ARs of the generalized fractal dimension D_0 and D_8 (top panels), and multifractal parameters $C_{\rm div}$ and $D_{\rm div}$ (bottom panels). Black and red symbols show results for the ARs in the northern and southern solar hemispheres, respectively.

McAteer, Gallagher, and Ireland (2005). They also show that depending on the analyzed ARs, the fractal and multifractal measurements derived from regions hosting distinct classes of events may have or may have not similar values, as reported from the analysis of two flaring and flare-quiet ARs by *e.g.* Georgoulis (2013) and by considering the results from the most flaring and most flare-quiet ARs in the sample analyzed in this study, respectively.

Table 3 lists the linear Pearson correlation coefficients between the measured parameters and FI. The absolute values of the coefficients derived by taking into account the parameters deduced from unsigned flux data of the analyzed ARs range from 0.51 to 0.60, being 0.51 (D_0), 0.60 (D_8), -0.55 ($C_{\rm div}$), and -0.52 ($D_{\rm div}$). These values confirm the weakly significant relation among the compared quantities already reported in the literature.

3.2. Average Values of the Parameters from Signed Flux Data

Figures 6 and 7 show the time series of fractal and multifractal parameters derived from signed flux measurements of the analyzed ARs. The regions were divided according to the three classes of flaring ARs mentioned above and depending on the hemisphere hosting the region, aiming at investigating potential

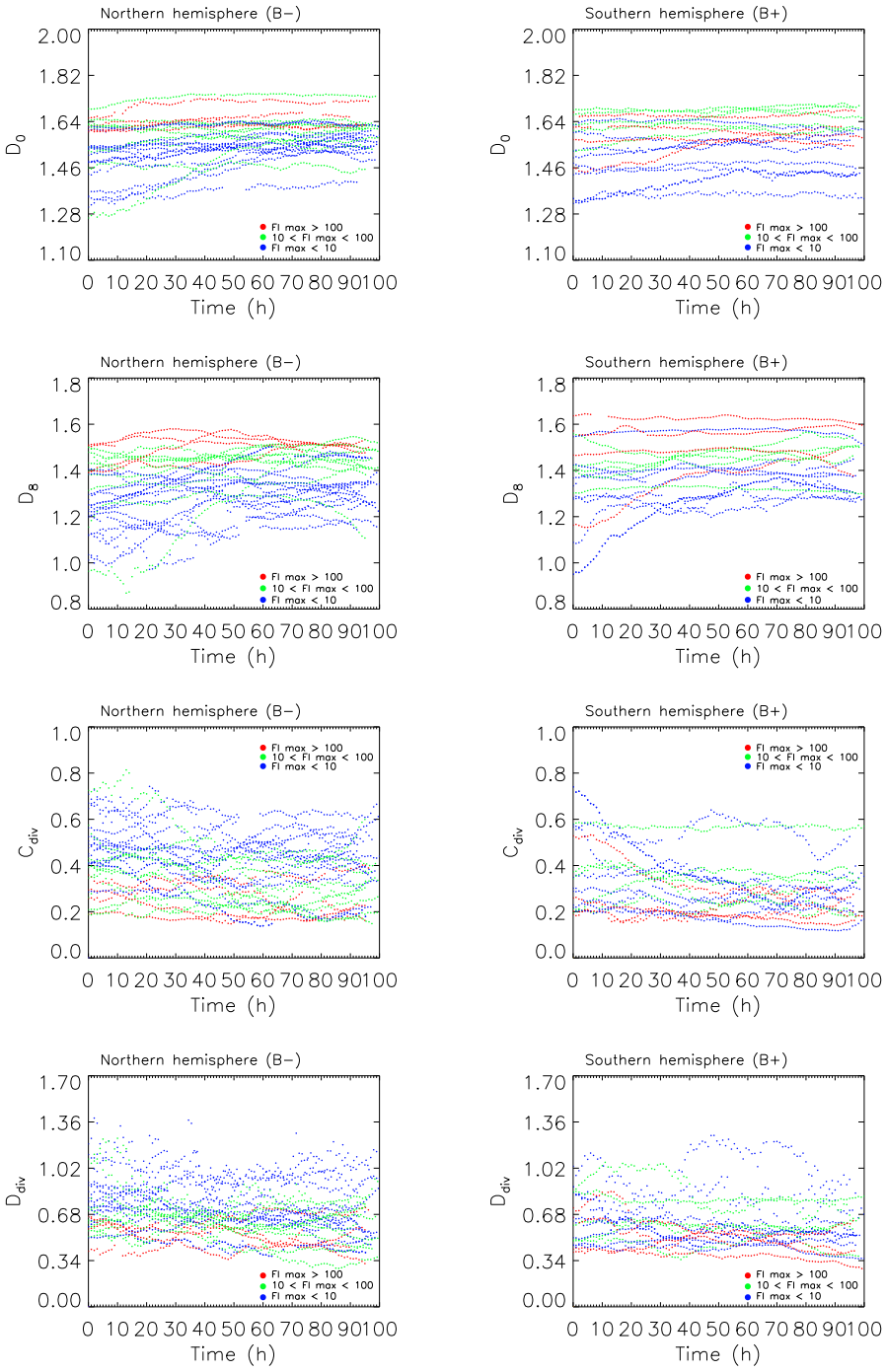

Figure 6. Comparison among results of the fractal and multifractal parameters measured on the whole sample of analyzed ARs. Time series of fractal (D_0 and D_8) and multifractal ($C_{\rm div}$ and $D_{\rm div}$) parameters. Shown are results from signed magnetic flux measurements of the leading polarity in the analyzed ARs that were divided according to their flaring level and the hemisphere hosting them, northern (left panels) and southern (right panels). For clarity, each symbol shows the average of results over 5 data points, which correspond to 1 h time interval. Legend as in Figure 3.

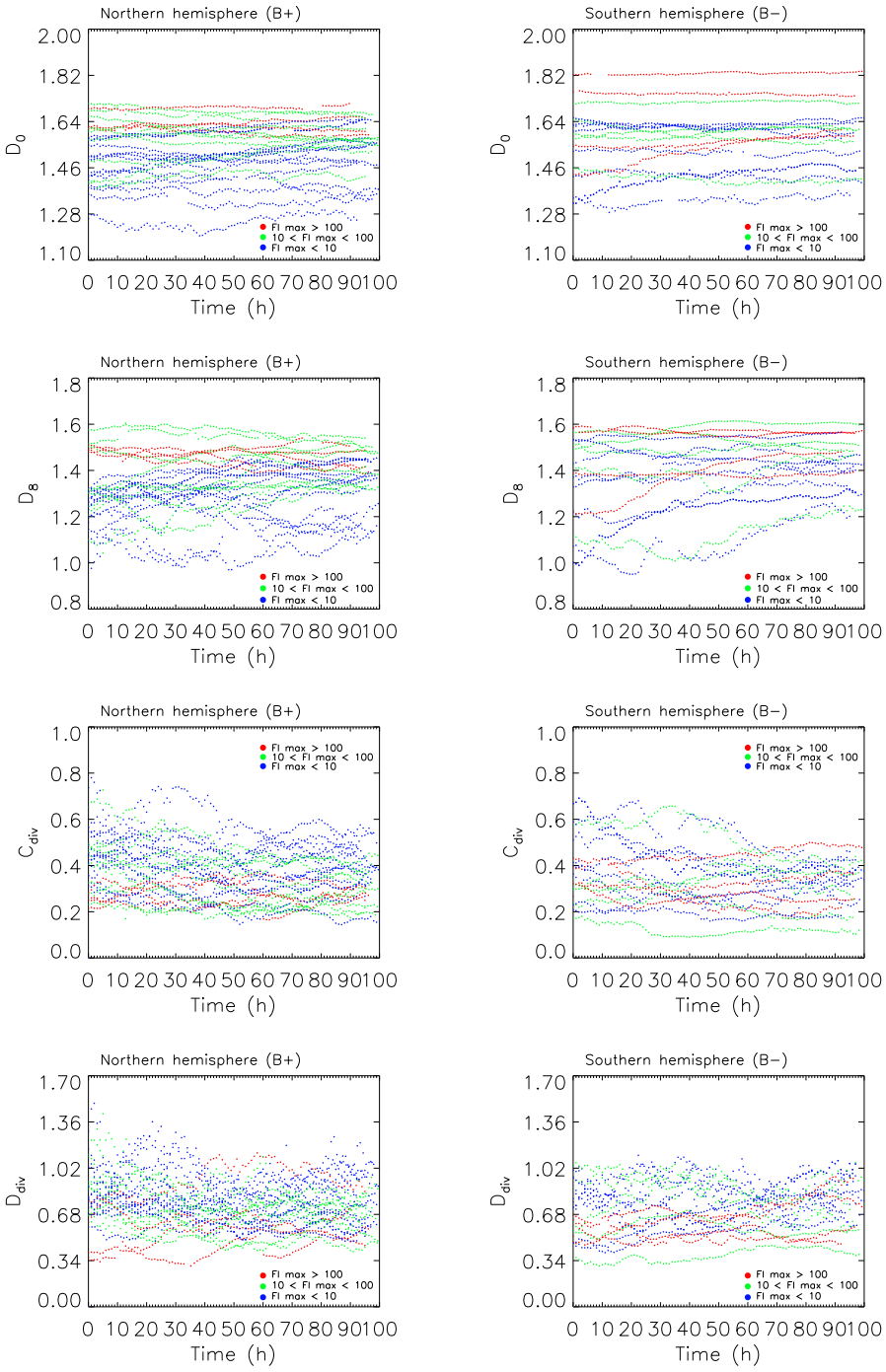

Figure 7. Comparison among results of the fractal and multifractal parameters measured on the whole sample of analyzed ARs. Time series of fractal (D_0 and D_8) and multifractal ($C_{\rm div}$ and $D_{\rm div}$) parameters. Shown are results from signed magnetic flux measurements of the trailing polarity in the analyzed ARs that were divided according to their flaring level and the hemisphere hosting them, northern (left panels) and southern (right panels). For clarity, each symbol shows the average of results over 5 data points, which correspond to 1 h time interval. Legend as in Figure 3.

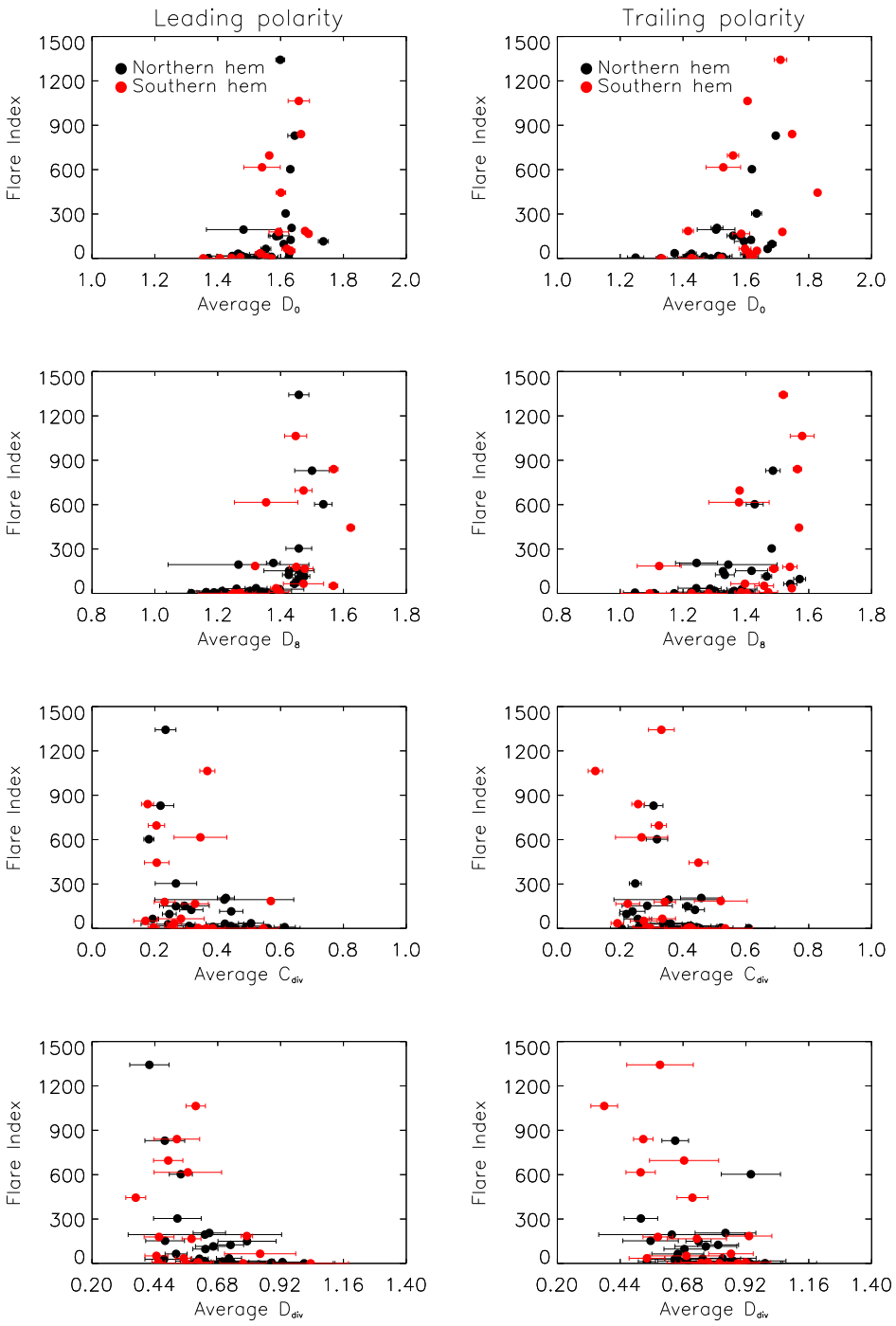

Figure 8. Flare index of the analyzed ARs versus average values of the fractal and multifractal parameters measured on our sample of 43 ARs, which includes B- or C-, M-, and X-class flaring regions. Shown are results from signed magnetic flux measurements of the leading (left panels) and trailing (right panels) polarity in the analyzed ARs of the generalized fractal dimension D_0 and D_8 and multifractal parameters $C_{\rm div}$ and $D_{\rm div}$. The ARs were divided according to hemisphere hosting them; black and red symbols show results for the ARs in the northern and southern hemispheres, respectively.

Table 2. Summary of the average value and standard deviation of the fractal (D_0 and D_8) and multifractal ($C_{\rm div}$ and $D_{\rm div}$) parameters measured in our sample of 43 ARs, which includes 8, 14, 16, and 5 regions that have produced at least one X-, M-, C, and B-class flare, respectively, by considering unsigned and signed flux data in the analyzed ARs, with distinction of the leading and following flux polarities in each AR.

Parameter	flux data	B and C flaring	M flaring	X flaring	All regions
D_0	unsigned	1.69± 0.06	1.77± 0.06	1.81±0.07	1.74±0.08
D_8	unsigned	1.35±0.09	1.45±0.07	1.54±0.06	1.42±0.11
$C_{\rm div}$	unsigned	0.58±0.07	0.54±0.06	0.47±0.03	0.55±0.08
$D_{\rm div}$	unsigned	0.88±0.16	0.80±0.13	0.65±0.05	0.81±0.15
D_0	leading polarity	1.51±0.08	1.61±0.07	1.61±0.04	1.57±0.10
D_8	leading polarity	1.30±0.10	1.41±0.07	1.50±0.08	1.37±0.12
$C_{\rm div}$	leading polarity	0.40±0.13	0.34±0.10	0.23±0.05	0.35±0.12
$D_{\rm div}$	leading polarity	0.71±0.18	0.64±0.12	0.49±0.06	0.66±0.17
D_0	trailing polarity	1.49±0.11	1.58±0.09	1.66±0.11	1.54±0.14
D_8	trailing polarity	1.31±0.13	1.40±0.14	1.47±0.07	1.37±0.14
$C_{\rm div}$	trailing polarity	0.38±0.11	0.33±0.11	0.31±0.06	0.36±0.11
$D_{\rm div}$	trailing polarity	0.78±0.13	0.71±0.14	0.64±0.14	0.74±0.14

Table 3. The linear Pearson correlation coefficients between the measured parameters and flaring level of the analyzed ARs, as expressed by their FI and FI max. The coefficients were computed by assuming measurement results from both unsigned and signed flux data in the analyzed ARs, with distinction of the leading and following flux polarities in each AR.

Flare index	flux data	D_0	D_8	$C_{\rm div}$	$D_{\rm div}$
FI	unsigned	0.51	0.60	-0.55	-0.52
FI	leading polarity	0.39	0.51	-0.39	-0.45
FI	trailing polarity	0.48	0.46	-0.33	-0.49
FI max	unsigned	0.48	0.53	-0.45	-0.44
FI max	leading polarity	0.32	0.48	-0.42	-0.43
FI max	trailing polarity	0.47	0.38	-0.20	-0.35

signatures on the measurements of the leading and trailing flux polarities in the studied ARs, as well as of the hemisphere hosting the regions. In this respect, it is worth noting that all analyzed ARs follow the main polarity orientation in the hemisphere, but AR NOAA 11429 that showed opposite polarity orientation than the other regions in the northern hemisphere.

For each AR, we found that the fractal D_0 values estimated on unsigned flux data are higher than those obtained by taking into account signed flux measurements in the same region, whereas the fractal D_8 and multifractal $C_{\rm div}$ and $D_{\rm div}$ values derived from the region do not vary significantly with the flux data employed to estimate the parameter.

We ascribe the distinct results obtained for the fractal parameter D_0 by taking into account unsigned and signed flux data to the different morphological configuration of magnetic flux concentration in an AR, by considering the region as a whole and its leading and following polarities separately. Indeed, observations (see *e.g.* Section 1 of Fan, 2009) show that the flux of the leading polarity in an AR tends to be concentrated in large well-formed sunspots, whereas the flux of the following polarity tends to be more dispersed and to have a fragmented appearance. At any finite spatial resolution, the latter implies lower average flux values measured in the analyzed region than actual ones and thus a higher sensitivity of morphological measurements based on flux data to threshold selection effects. We found signatures in our measurements of these observational evidences in *e.g.* the lower average values of the parameters derived from signed flux data with respect to results from unsigned data, as well as of the values from the trailing polarity in the analyzed ARs, with respect to the values obtained from the data of the leading polarity flux in the ARs. The lower sensitivity of the fractal D_8 and multifractal $C_{\rm div}$ and $D_{\rm div}$ measurements on the flux data employed for the study than obtained from D_0 suggests us that measurements of the former parameters on signed flux data may benefit from analysis of higher resolution observations than employed in this study. In fact, the former parameters, by corresponding to a higher order estimates of the fractal dimension than D_0, may require larger data set to allow similar statistical significance of results than obtained for D_0.

Figure 8 shows the relation between the average values of the parameters estimated by taking into account the signed flux data of each analyzed AR and its FI. The results in this Figure confirm the findings derived from the measurements of the parameters based on unsigned flux data of the analyzed ARs. In particular, they confirm both the weak relation between the compared quantities and lack of distinctive hemispheric signatures on the measurements.

Tables 2 and 3 quantify the results discussed above. In particular, the average and standard deviation of values measured by discriminating the flux data in the analyzed ARs reported in Table 2, as well as the Pearson correlation coefficients between the measured values and FI of the analyzed ARs listed in Table 3, confirm previous conclusions by Georgoulis (2005) on that discriminating between the flux polarities in the ARs do not alter the results derived from analysis of total unsigned flux data of the regions. Indeed, in this study, the lower values obtained for the Pearson coefficients of the parameters based on signed flux data in the analyzed ARs show that discriminating between the flux polarities has even reduced the weak correlation between the compared quantities, with respect to results based on unsigned flux data of the ARs.

3.3. Temporal Evolution of the Parameters

We then focussed our attention on the temporal evolution of the various parameters measured on the whole sample of analyzed ARs, aiming at identifying any clear patterns on the parameter series that can be associated with the flare activity of the ARs. Here in the following the term variation indicates the deviation of measured values with respect to the average and long-term trends of the

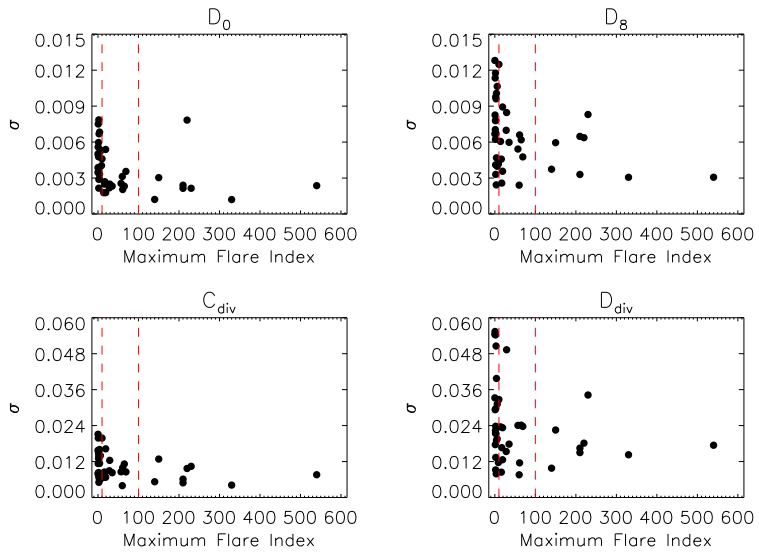

Figure 9. Variance of the distribution of the fractal and multifractal parameters measured on each region versus the maximum flare index of the studied AR. The parameter values refer to the deviation of measurement results with respect to the average trend of the parameter that was obtained with a running average of the values measured over a 3 h time interval. Shown are results from unsigned magnetic flux measurements in the ARs of the generalized fractal dimension D_0 and D_8 (top panels), and multifractal parameters $C_{\rm div}$ and $D_{\rm div}$ (bottom panels). The ARs were divided into three classes (vertical dashed lines), depending on the value of their maximum flare index.

parameters. These trends were defined as specified in the following. The variation of measured values has been quantified by the variance of the distribution of measured values, as well as by the distinct patterns identified on the analyzed series.

First, we studied the distribution of parameter values measured for each region during its transit over the solar disc and the dependence of the distribution variance σ on the flaring activity of the AR. In particular, we computed the distribution of parameter values measured for each region with respect to the average and longer-term trends of the parameters, which were obtained with a running average of values measured over 3 and 12 h time interval, respectively. We then estimated the width of the Gaussian function that best fits the measured distribution and assumed this width as an estimate of the distribution variance σ.

Figure 9 shows the σ measured for each AR in the analyzed sample with respect to its FI max. We found that the distribution of values derived from the less flaring regions are characterized by a larger variance with respect to the ones obtained from the more flaring ARs. However, the variance of the values derived from all analyzed ARs does not show any clear dependence on the flaring activity of the regions, by disclaiming the idea that more flaring ARs may leave the signature of their activity in more varying time series of the measured parameters. This result holds likewise for the variance of the values

measured with respect to both the average and longer-term trends of measured values.

We then analyzed the time series derived from each AR and their main features. A sample of the analyzed data has been already shown in Figures 1 and 2. We found that the time series of the D_0 and D_8 fractal parameters measured on the whole sample of ARs show smaller and more regular variations during the analyzed time intervals than the corresponding trends of the $C_{\rm div}$ and $D_{\rm div}$ multifractal values. This holds for results derived from both unsigned and signed flux data in the studied ARs. We found that D_8 shows slightly larger changes than D_0, as $D_{\rm div}$ also does with respect to $C_{\rm div}$, and particularly when results obtained from signed flux data are taken into account. This result suggests us that measurements of these parameters on signed flux data may benefit from analysis of higher resolution data than employed in this study.

We also found that most of the studied series show different evolution during the analyzed time intervals depending on the flux data employed to estimate the parameters. In particular, we found that the time series of the parameters derived from a given field polarity are less consistent with those obtained from unsigned flux data on the same regions, which resulted to be rather representative of the parameter trends deduced from the opposite flux polarity in the ARs. Specifically, the most varying trends for all measured parameters were found to be the ones deduced from the trailing flux data of the analyzed ARs, i.e. the data of the flux concentration with higher fragmentation and thus also higher sensitivity of measurement results to the finite spatial resolution of the analyzed data. The trends of the parameter estimates based on the prevailing leader polarity in the hemisphere hosting the AR were found to be more consistent with those obtained from unsigned flux data. These features of the time series, specifically the similarity between the trends deduced from unsigned and leading polarity flux of the analyzed ARs and the deviation between the same trends and those from the trailing polarity flux, were found to hold for $\approx 90\%$ of the studied regions. It is worth noting that the parameter time series of AR NOAA 11429, which is the only region in the analyzed data set that showed opposite polarity orientation than the other regions, do no follow the results derived from most of the data analyzed.

From analysis of the parameter series we also found that several flares occur during a decreasing phase of the$D_{\rm div}$ and an increasing phase of the D_8 values estimated by considering unsigned and signed flux data of the leading polarity of the AR hemisphere. However, those features of the parameter trends were not found to be a consistent pre-flare signature on the whole sample of ARs and events. Indeed, this event signature was found on $\approx 50\%$ of the analyzed ARs and on $\approx 50\%$ of the $\geq$ M-class events considered. We also found that the$D_{\rm div}$ trends obtained by considering the trailing polarity of the ARs show changes lasting few hours (< 10) and occurring both prior (≈ 15 h) and after major events, as shown in Figure 2 for *e.g.* AR 11158 and AR 11875, where B- and B+ is the trailing polarity in the region, respectively. These changes in $D_{\rm div}$, whose amplitude ranges 0.20% to 0.25% of the parameter value independently of the event class, are compatible with a simplification of the photospheric magnetic field in flaring ARs through sudden changes of the trailing flux topology. However, they were found on $\approx 50\%$ of the analyzed ARs and events.

4. Conclusion

The present study shows that the analysis of a large data set of higher spatial and temporal resolution, as well as higher flux sensitivity, observations than employed in previous studies does not give the fractal and multifractal parameter measurements a higher efficiency to discriminate ARs depending on their flaring activity than reported in the literature. The measurements derived from our study hint to a signature of the flare activity in the fractal and multifractal parameters of ARs and a potential differentiation depending on their flare activity, but this does not hold in general for all the analyzed ARs. In particular, we found distinct average values of the parameters measured on ARs that have hosted flares of different class, in agreement with the statistical trend reported by McAteer, Gallagher, and Ireland (2005). At a first glance, our findings contrast with results presented by *e.g.* Georgoulis (2013). However, we also show that the dispersion of values deduced from each class of flaring AR considered in our study is such that results from extreme classes of flaring ARs can also overlap, as shown in *e.g.* Figure 8 of Georgoulis (2013).

The results obtained by our study also show that the parameter estimates based on signed flux measurements do not constitute a better predictive tool of the flare activity than derived by using unsigned flux data as in previous studies. In particular, we found that the time series of the parameters obtained from unsigned flux data of the analyzed ARs are rather representative of those deduced from the signed flux measurements of the prevailing leader polarity in the hemisphere hosting the ARs. Both time series show that the flares occur during a decreasing phase of the$D_{\rm div}$ and an increasing phase of the D_8 parameters on $\approx$ 50% of the analyzed ARs and on $\approx$ 50% of the $\geq$ M-class events considered. The times series of parameters deduced from signed flux data of the trailing polarity flux in the analyzed ARs are less consistent with those derived from unsigned flux data of the studied region. The former time series show changes of the evolution of the $D_{\rm div}$ values lasting few hours and occurring both prior and after major events. These changes, which are compatible with a simplification of the magnetic field in the ARs, were found on $\approx$ 50% of the analyzed regions and events.

The results obtained in this study give reasons to the conflicting conclusions reported in the literature on the efficiency of the fractal and multifractal parameter measurements based on unsigned flux data of ARs to discriminate them depending on their flaring activity. They also extend the validity of the previous findings to results derived from signed flux measurements of the analyzed ARs. It remains to be shown whether other parameters describing the magnetic field evolution and morphological complexity based either on signed or other flux data of the analyzed regions prove to be more ideal tools for discriminating flaring ARs than those analyzed in this study.

Acknowledgements The research leading to these results has received funding from the European Commission's Seventh Framework Programme (FP7/2007-2013) under the grant agreements eHEROES (project n 284461, www.eheroes.eu) and SOLARNET (n 312495, www.solarnet-east.eu). This work was also supported by the Istituto Nazionale di Astrofisica (PRIN-INAF-

2010). The authors acknowledge useful discussions from Giuseppe Consolini and Gherardo Valori.

References

Abramenko, V.I.: 2005, Multifractal analysis of solar magnetograms. *Solar Phys.* **228**, 29 – 42. doi:10.1007/s11207-005-3525-9.

Barnes, G., Leka, K.D.: 2008, Evaluating the performance of solar flare forecasting methods. *Astrophys. J. Lett.* **688**, L107 – L110. doi:10.1086/595550.

Burtseva, O., Petrie, G.: 2013, Magnetic flux changes and cancellation associated with X-class and M-class flares. *Solar Phys.* **283**, 429 – 452. doi:10.1007/s11207-013-0241-8.

Cliver, E.W., Petrie, G.J.D., Ling, A.G.: 2012, Abrupt changes of the photospheric magnetic field in active regions and the impulsive phase of solar flares. *Astrophys. J.* **756**, 144. doi:10.1088/0004-637X/756/2/144.

Conlon, P.A., Gallagher, P.T., McAteer, R.T.J., Ireland, J., Young, C.A., Kestener, P., Hewett, R.J., Maguire, K.: 2008, Multifractal properties of evolving active regions. *Solar Phys.* **248**, 297 – 309. doi:10.1007/s11207-007-9074-7.

Criscuoli, S., Rast, M.P., Ermolli, I., Centrone, M.: 2007, On the reliability of the fractal dimension measure of solar magnetic features and on its variation with solar activity. *Astron. Astrophys.* **461**, 331 – 338.

Criscuoli, S., Romano, P., Giorgi, F., Zuccarello, F.: 2009, Magnetic evolution of superactive regions. Complexity and potentially unstable magnetic discontinuities. *Astron. Astrophys.* **506**, 1429 – 1436.

Ermolli, I., Giorgi, F., Romano, P., Zuccarello, F., Criscuoli, S., Stangalini, M.: 2014, Fractal and multifractal properties of active regions as flare precursors: A case study based on SOHO/MDI and SDO/HMI observations. *Solar Phys.* **289**, 2525 – 2545. doi:10.1007/s11207-014-0500-3.

Fan, Y.: 2009, Magnetic fields in the solar convection zone. *Living Rev. Solar Phys.* **6**(4). doi:10.12942/lrsp-2009-4.

Georgoulis, M.K.: 2005, Turbulence in the solar atmosphere: Manifestations and diagnostics via solar image processing. *Solar Phys.* **228**, 5 – 27. doi:10.1007/s11207-005-2513-4.

Georgoulis, M.K.: 2012, Are solar active regions with major flares more fractal, multifractal, or turbulent than others? *Solar Phys.* **276**, 161 – 181. doi:10.1007/s11207-010-9705-2.

Georgoulis, M.K.: 2013, Toward an efficient prediction of solar flares: Which parameters, and how? *Entropy* **15**, 5022 – 5052. doi:10.3390/e15115022.

Giannattasio, F., Stangalini, M., Del Moro, D., Berrilli, F.: 2013, On the asymmetry of velocity oscillation amplitude in bipolar active regions. *Astron. Astrophys.* **550**, A47. doi:10.1051/0004-6361/201220103.

Hapgood, M.: 2012, Astrophysics: Prepare for the coming space weather storm. *Nature* **484**, 311 – 313. doi:10.1038/484311a.

Leka, K.D., Barnes, G.: 2013, Solar flare forecasting: A "state of the field" report for researchers. In: *Bull. Am. Astron. Soc.* **45**, 100.82.

Li, Y., Luhmann, J., Fisher, G., Welsch, B.: 2004, Observational evidence for velocity convergence toward magnetic neutral lines as a factor in CME initiation. *J. Atmos. Solar-Terr. Phys.* **66**, 1271 – 1282. doi:10.1016/j.jastp.2004.03.017.

McAteer, R.T.J., Gallagher, P.T., Ireland, J.: 2005, Statistics of active region complexity: A large-scale fractal dimension survey. *Astrophys. J.* **631**, 628 – 635. doi:10.1086/432412.

Romano, P., Zuccarello, F.: 2011, Flare occurrence and the spatial distribution of the magnetic helicity flux. *Astron. Astrophys.* **535**, A1. doi:10.1051/0004-6361/201117594.

Sammis, I., Tang, F., Zirin, H.: 2000, The dependence of large flare occurrence on the magnetic structure of sunspots. *Astrophys. J.* **540**, 583 – 587. doi:10.1086/309303.

Scherrer, P.H., Bogart, R.S., Bush, R.I., Hoeksema, J.T., Kosovichev, A.G., Schou, J., Rosenberg, W., Springer, L., Tarbell, T.D., Title, A., Wolfson, C.J., Zayer, I., MDI Engineering Team: 1995, The Solar Oscillations Investigation - Michelson Doppler Imager. *Solar Phys.* **162**, 129 – 188. doi:10.1007/BF00733429.

Scherrer, P.H., Schou, J., Bush, R.I., Kosovichev, A.G., Bogart, R.S., Hoeksema, J.T., Liu, Y., Duvall, T.L., Zhao, J., Title, A.M., Schrijver, C.J., Tarbell, T.D., Tomczyk, S.: 2012, The Helioseismic and Magnetic Imager (HMI) investigation for the Solar Dynamics Observatory (SDO). *Solar Phys.* **275**, 207 – 227. doi:10.1007/s11207-011-9834-2.

Schou, J., Scherrer, P.H., Bush, R.I., Wachter, R., Couvidat, S., Rabello-Soares, M.C., Bogart, R.S., Hoeksema, J.T., Liu, Y., Duvall, T.L., Akin, D.J., Allard, B.A., Miles, J.W., Rairden, R., Shine, R.A., Tarbell, T.D., Title, A.M., Wolfson, C.J., Elmore, D.F., Norton, A.A., Tomczyk, S.: 2012, Design and ground calibration of the Helioseismic and Magnetic Imager (HMI) instrument on the Solar Dynamics Observatory (SDO). *Solar Phys.* **275**, 229 – 259. doi:10.1007/s11207-011-9842-2.

Wachter, R., Schou, J., Rabello-Soares, M.C., Miles, J.W., Duvall, T.L., Bush, R.I.: 2012, Image quality of the Helioseismic and Magnetic Imager (HMI) onboard the Solar Dynamics Observatory (SDO). *Solar Phys.* **275**, 261 – 284. doi:10.1007/s11207-011-9709-6.

Yamamoto, T.T.: 2012, The area asymmetry in bipolar magnetic fields. *Astron. Astrophys.* **539**, A13. doi:10.1051/0004-6361/201014951.

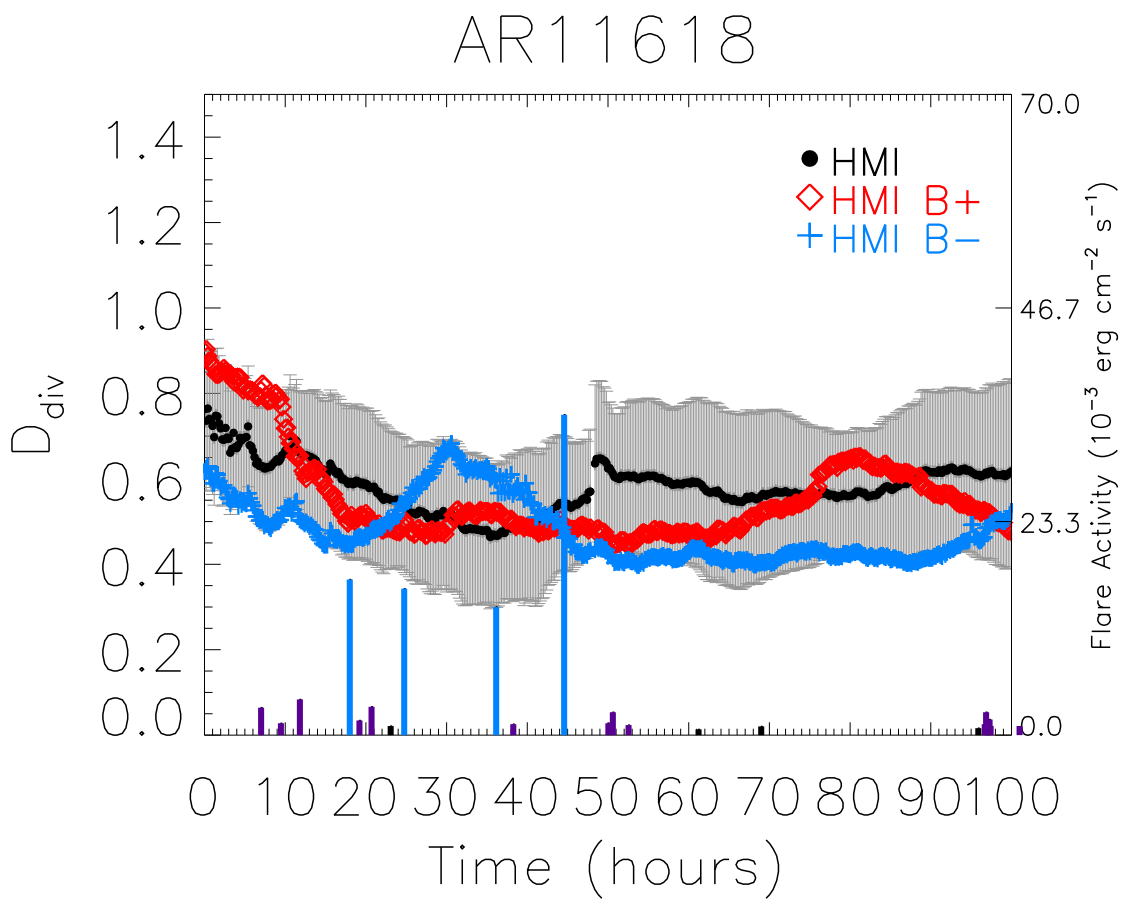
AR11618
HMI
HMI B+
HMI B−
D_{div}
1.4
1.2
1.0
0.8
0.6
0.4
0.2
0.0
70.0
46.7
23.3
0.0
Flare Activity (10^{-3} erg cm^{-2} s^{-1})
0 10 20 30 40 50 60 70 80 90 100
Time (hours)

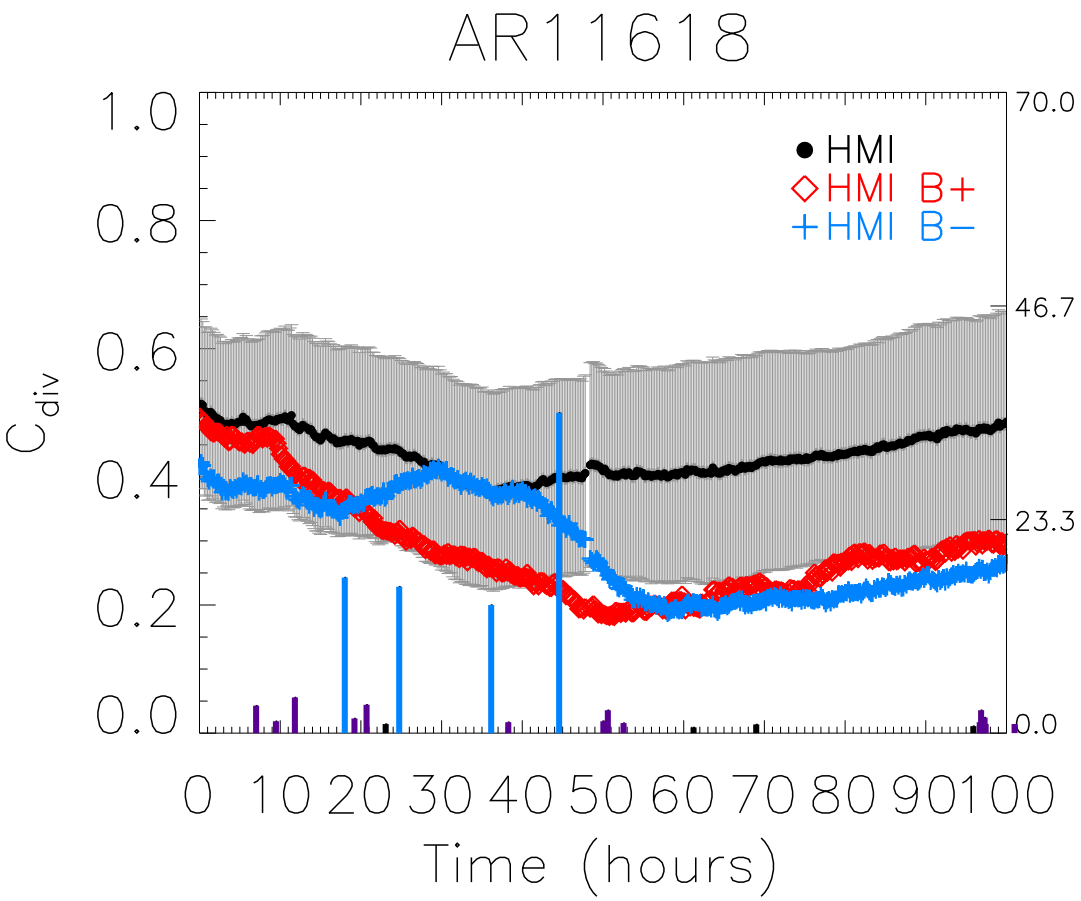
AR11618
1.0
0.8
0.6
0.4
0.2
0.0
C_{div}
HMI
HMI B+
HMI B−
70.0
46.7
23.3
0.0
0 10 20 30 40 50 60 70 80 90 100
Time (hours)